Spatial PSF Non-Uniformity Effects In Airborne Pushbroom Imaging Spectrometry Data

Daniel Schläpfer, Jens Nieke, and Klaus I. Itten, *Member, IEEE*

Abstract—Efficient and accurate imaging spectroscopy data processing asks for perfectly consistent (i.e., ideally uniform) data in both the spectral and the spatial dimension. However, real pushbroom type imaging spectrometers are affected by various Point Spread Function (PSF) non-uniformity artefacts: first, individual pixels or lines may be missing in the raw data due to bad pixels originating from the detector, readout errors, or even electronic failures. Secondly, so-called smile and keystone optical aberrations are inherent to imaging spectrometers. Appropriate resampling strategies are required for the preprocessing of such data if emphasis is put on spatial PSF uniformity. So far, nearest neighbor interpolations have been often recommended and used for resampling. This paper shall analyze the radiometric effects if linear interpolation is used to optimize the spatial PSF uniformity. For modeling interpolation effects, an extensive library of measured surface reflectance spectra as well as real imaging spectroscopy data over various land cover types are used. The real measurements are systematically replaced by interpolated values and the deviation between original and resampled spectra is taken as a quality measure. The effects of nearest neighbor resampling and linear interpolation methods are compared. It is found that linear interpolation methods lead to average radiometric errors below 2% for the correction of spatial PSF non-uniformity in the sub-pixel domain, whereas the replacement of missing pixels leads to average errors in the range of 10-20%.

Index Terms—Remote Sensing, Imaging Spectroscopy, Interpolation, Uniformity

I. INTRODUCTION

PUSHBROOM type imaging spectrometers offer advantages in robustness, integration time, speed, and spectral/spatial resolution. Unfortunately, the Point Spread Function (PSF) [1] uniformity of such data is often a major issue in data preprocessing and analysis. Expected PSF non-uniformities in the spatio-spectral frames of a pushbroom imaging spectrometer are so-called keystone and smile effects [2], spatial mis-registration between detector arrays, as well as malfunctioning detector pixels. The spatial co-registration of

all image pixels between detector arrays is critical for pushbroom instruments covering the typical spectral range between 400 and 2500 nm wavelength, as this range is usually covered by more than one detector array. Furthermore, smile and keystone effects are present due to sub-pixel optical aberrations and sampling inconsistencies in the spectral and the spatial domain, respectively. All these effects lead to radiometric inconsistencies (i.e., non-uniformities) in the imaging spectrometry data.

The uniformity of imaging spectroscopy data shall be improved by selecting the appropriate corrections scheme for PSF non-uniformities inherent to any sensor system. Correction strategies to improve the uniformity (and to ease the subsequent data processing) are being developed [3][4], but such procedures are not always systematically applied in the calibration process of airborne imaging spectroscopy data. Considerable effort has been done so far for optimizing the uniformity of data stemming from space borne systems such as from the Medium Resolution Imaging Spectrometer (MERIS) [5],[6] and from the Moderate Resolution Imaging Spectroradiometer (MODIS) [7]. Analyzing and correcting non-uniformity effects is also critical for Hyperion [8] or (e.g.) the Compact Airborne Spectrographic Imager (CASI) [9]. Note that the effects of non-uniform spatial PSFs are more pronounced for airborne imaging spectrometers with unstable platforms in combination with a high spatial resolution, as the platform motion increases the effects of non-uniformity in the registered data.

It is known that standard interpolation routines are suitable to resample mis-registration artefacts, which has been studied in depth over the last two decades for multispectral remote sensing data [10]. Also, the interpolation methods have evolved and a broad variety of interpolation options are available in modern imaging processing systems [11]. However, the impact of interpolation on the accuracy of a continuous spectrum is seldomly described in literature. Yet to be evaluated is the degree to which the spatial mis-registration influences the radiometric quality of the data and which strategies are best suited to improve the overall data quality.

Some comments about the terminology used as well as an overview of resampling strategies are given hereafter. The impact of resampling algorithms principally has to be evaluated in both the spectral and the spatial dimension. This paper will focus on the effects of spatial PSF non-uniformities

on the spectroradiometric measurements, whereas the spectral PSF non-uniformities are omitted. The intention is to quantify the errors related to spatial PSF non-uniformities and to provide data suitable for a trade off between spatial PSF uniformity gain and spectroradiometric information loss.

This work is done in preparation of the airborne imaging spectrometer APEX (Airborne Prism EXperiment) which is currently being built in a joint Swiss/Belgium project funded through the European Space Agency (ESA) [12], [13]. This instrument is constructed as an airborne dispersive pushbroom instrument having 1000 pixels across track and up to 511 spectral bands registered simultaneously on two distinct detector arrays. The instrument's concept allows for a (relatively) high resolution in both the spectral and the spatial domain. A high radiometric quality of the instrument's outputs is a major task to be accomplished [14] and, thus, the optimization of uniformity of its data is a key issue in the development process of its processing and archiving facility (PAF) [15], [16].

II. TERMS AND DEFINITIONS

The terminology for the description of uniformity is not fully consistent throughout literature. The goal of this work is to quantify the impact of the spatial PSF non-uniformity for data processing. Therefore, the definitions focus on the description of effects in the imaging spectroscopy data cube. The dimensions of a 3-dimensional imaging spectroscopy cube correspond to the parameters time, central wavelength position, and across track view angle. The response curves in these three directions are associated in a 1:1 manner for each pixel, being constant within the required accuracy with respect to the non-associated dimension (e.g., the spectral response shall be constant with time and across track view angle). These rules may be violated by various artefacts which leads to non-uniform image data. The term 'artefact' is used herein for any kind of inconsistency (non-uniformity) in pushbroom imaging spectroscopy data. Two uniformity terms are commonly used for the description of artefacts in electronic imaging:

Spatial uniformity is the radiometric response equality within a (spatial) frame detector. This term primarily stems from frame imaging, e.g. in medical applications [17], [18]. It includes effects such as striping or spectrally variable radiometric response related to changing quantum efficiency.

Temporal uniformity is the temporal radiometric response stability of a detector element. This term is common in video analysis [19], and is used synonymously with 'radiometric stability' in imaging spectroscopy.

For pushbroom imaging spectroscopy, one image frame registers the spectral and the spatial dimension simultaneously. Any non-uniformity in the system PSF leads therefore to the following artefacts [2]:

Spectral PSF uniformity is the equality of the spectral response (i.e., spectral PSF) within a sensors spectral band and is usually imaged on a detector row. This uniformity is typically described by position ('*Spectral uniformity*') and shape of the spectral response function. The related artefacts

of spectral mis-registration are hereafter also denoted as '*smile*'.

Spatial PSF uniformity is the equality of the spatial response (i.e., spatial PSF) within an acquired spectrum and is usually imaged on a detector column. This uniformity is described by position and shape of the spatial response function in both the along track and the across track dimensions of a spatial pixel. The related artefacts of spatial mis-registration in the across track dimension are hereafter also denoted as '*keystone*'.

Assuming a Gaussian shape of the response functions, the position is parametrized by the local maximum response, while the width is usually measured at 'full width at half maximum' (FWHM). The characteristics of the spectral or the spatial PSF may vary either by the position of the PSF as well as by its width. This fact leads to six sub-categories of non-uniformities: spectral band position uniformity, spectral width uniformity, spatial across track position uniformity, spatial across track width uniformity, spatial along track position uniformity, and spatial along track width uniformity.

In this paper, the PSF effects affecting uniformity of a spectrum in the spatial domain (i.e., the spatial PSF uniformity) are investigated. Spectral PSF uniformity artefacts are not analyzed at this place although their impact on the data quality is on the same order of magnitude as for the spatial dimension since both dimensions are registered on the same detector array. Nevertheless, de-coupling of the two dimensions makes sense, insofar that the two dimensions 'wavelength' and 'space' are physically different.

III. SPATIAL PROCESSING ALGORITHMS

Remote sensing data corrections in the spatial domain (i.e., spatial resampling algorithms) are well known for image registration and rectification processes [20]. The corresponding resampling procedures on the image level are comparable to the correction of keystone effects on the detector level, as both processing steps affect the spatial dimension of the imagery and are usually to be performed within a distance of 0.1 to 2 pixels. One main precondition for successful resampling is that the data of the whole image frame is radiometrically corrected and calibrated to physical units (i.e., radiance [W/(m^2 sr nm)]). After this data calibration step, it must be determined how much and which kind of uniformity is most important for derivation of the specific imaging spectroscopy products.

Nearest neighbor techniques have been proposed and often applied for replacements of missing measurements in imaging spectroscopy data (e.g., for MERIS [6] or AVIRIS [21]). The nearest neighbor resampling avoids any interpolation and thus the full information content of the spectra can be preserved. The problem of applying nearest neighbor techniques is a loss in spatial registration accuracy, since the spectra are simply shifted in their spatial position. Other resampling strategies are required as soon as the spatial PSF uniformity is to be corrected or if registration accuracy is of higher relevance. Extensive studies for the spatial effects of

resampling on images have been done earlier with respect to spatial accuracy considerations [22], [10], [23]. However, the influence of the spatial PSF non-uniformity was not of major concern in these studies. In the spectral domain, the major point of concern has been the treatment of bandwidth variations [24] or the correction for spectral smile effects in band center position [25]. This topic has become a major concern for the preprocessing of Hyperion imagery [26].

A known variety of interpolation methods are routinely used for image processing [1] and for GIS applications [27]; the basic methods are summarized below.

A. Nearest Neighbor Resampling

The interpolated pixel value is transferred from the nearest pixel position as:

$$L_i(x_p, y_p) = L(x_p + \Delta x, y_p + \Delta y), \qquad (1)$$

where $L_i(x_p, y_p)$ is the re-located radiance at the final pixel position (x_p, y_p), L is the original radiance value, and Δx and Δy are the distances to the selected nearest neighbor, where $\sqrt{\Delta x^2 + \Delta y^2}$ is the minimal distances to the selected position.

B. Linear Interpolation

A computationally fast linear interpolation can be performed by averaging the linear interpolates of the two spatial image dimensions such that:

$$L_i(x_p, y_p) = \left(L(x)_{xp} + L(y)_{yp} \right)/2, \qquad (2)$$

where $L(x)_{xp}$ and $L(y)_{yp}$ are the linearly interpolated continuous functions of radiance in across track and along track directions, respectively. This approach does not include a full consideration of the relative distances of the pixels and thus may lead to artefacts whenever the interpolation distance is more than the size of one pixel.

C. Bilinear Interpolation

Triangulation has proven to provide an accurate representation of surface patterns as seen in remote sensing data. Thus, an accurate bilinear interpolation is done by triangulating before interpolating. The interpolation is afterwards done by gridding the triangulated surface $L(x, y)_{triang}$ to a uniform target raster, where the interpolated value is found as:

$$L_i(x_p, y_p) = L(x, y)_{triang}\big|_{xp, yp}, \qquad (3)$$

which represents a two-dimensional (i.e., bilinear) interpolation from the three closest original data points.

D. Advanced Resampling Algorithms

A number of more sophisticated resampling methods have been proposed and successfully applied to remote sensing data in the last decades [11], [28], [29]. They include cubic convolution [30], radial basis functions [31], spline interpolations [32], and neural network based processing [33]. Such advanced resampling algorithms are not further evaluated in this paper since it was a goal to investigate the influence of interpolation routines in general on the spectroradiometric accuracy if compared to the nearest neighbor technique. Using bilinear interpolation as the standard approach increases the observed error levels slightly, but leads to valid conclusions on the relative differences between various resampling strategies. The second reason for this constraint is the extensive computing time requirements for most of the advanced resampling strategies which makes them impractical for operational preprocessing of imaging spectroscopy data. Extensive validation results for the various resampling methods can be found in the above-mentioned references.

IV. Reference Data Basis

The error introduced by resampling techniques shall be quantified using existing high quality imaging spectroscopy data. For the purpose of this paper, data of a whiskbroom sensor has been selected since the uniformity of these systems is substantially higher than any current pushbroom sensor (see e.g. AVIRIS [34] validation results). Non-uniformity artefacts can then be simulated on realistic data structures without interfering with data-intrinsic non-uniformities. Secondly, a representative collection of high quality field spectra is taken as a reference of surface reflectance spectral variability.

A. Imaging Spectroscopy Data

A set of ten exemplary data sets from the AVIRIS sensor [34] has been selected for a realistic imaging spectroscopy data representation. Both, low and high altitude data have been engaged as summarized in Table I. The represented exemplary surface cover types are desert, mining, scattered vegetation, agriculture, forestry, city, and settlement (compare Figure 1).

TABLE I
DATA BASIS FOR SPATIAL RESAMPLING ANALYSIS WITH GEOMETRIC DESCRIPTION (GSD: GROUND SAMPLING DISTANCE, PSF: APPROXIMATIVE GEOMETRIC POINT SPREAD FUNCTION AT FWHM).

	Years	GSD	PSF	Remarks
AVIRIS low altitude	1998 - 2001	3.6 m	5 m	high resolution
AVIRIS high altitude	1998 / 2000	20.2 m	28.3 m	low resolution
APEX (project)	*2007*	*1.7-5 m*	*2-6 m*	*in development*

The data sets are chosen with typical but very distinct surface cover characteristics. Half of the scenes represent natural landscape of scattered patterns with little human influence, while the other half covers human-shaped areas. Calibrated at-sensor radiance image data is used for the analysis as interpolations are potentially biased if done on uncalibrated data. No geometric correction is applied in order to preserve the original statistical distribution of the single spectral measurements. The SNR values of AVIRIS range approximately between 100 and 300 if radiance levels are scaled to a typical land surface [34] which results in an uncertainty below 1% of this basis data set.
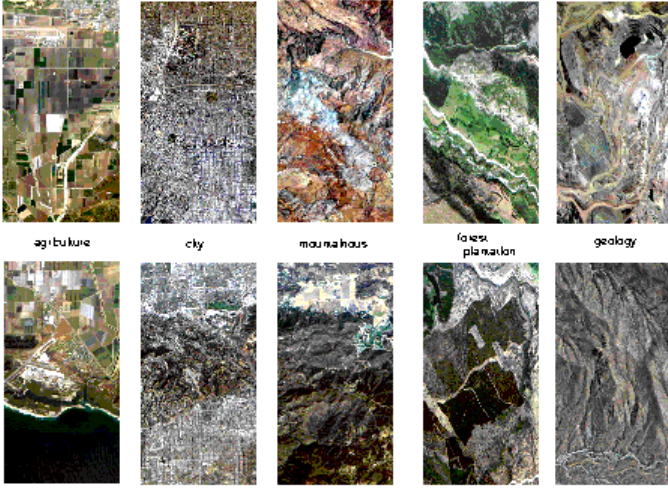
Fig. 1. Collection of realistic test data sets: ten exemplary AVIRIS scene subsets; 6 high altitude (left images; spatial resolution ~20 m) and 4 low altitude samples (right images; spatial resolution ~4 m).

B. Spectrum Reference Database Cube

The second data set engaged is an artificial test data set. A spectral data cube has been derived from the SPECCHIO spectral database [35]. The database includes a wide representative range of more than 4000 natural and simulated surface reflectance spectra. The data has been modeled to at-sensor radiance data using the MODTRAN4 radiative transfer code [36] at standard atmospheric parameters: flight altitude 7.5 km, ground elevation 0.2 km, midlatitude summer atmosphere, rural aerosols (23 km visibility), and the solar zenith at 22 degrees. These results were ordered in two complete spectral data cubes at 1-2 nm spectral sampling interval, resulting in 1391 bands between 370 and 2520 nm (see Figure 2). Each spectrum is repeated in the cube within an area of 3x3 or (in the second cube) at 5x5 pixels, forming a regular grid of spectral patches, suited for subsequent interpolation. For later PSF analyses, this data is convolved to the APEX specifications, reducing the number of bands to 313.

Fig. 2. Spectral database based artificial image (1000x120 pixels, 1391 spectral bands), in a thematically ordered spatial structure. Each visible spatial element represents one spectrum of the database in a 5x5 pixels square.

V. SIMULATION OF PSF NON-UNIFORMITY EFFECTS

Three non-uniformity effects are simulated using the above described test data sets: spatial discontinuities (missing pixels), spatial PSF width non-uniformity, and spatial PSF position non-uniformity. Results of the analyses are summarized hereafter, while some recommendations for the correction of such artefacts are given in Section VI.

A. Spatial Discontinuity Effects

It is tested how the correction of spatial discontinuities [37] (i.e., missing pixels) affects the image quality. A method

based on the real data sets has been chosen for proper representation of the errors involved with spatial resampling. Four types of spatial masks are created which represent missing individual pixels, missing lines (i.e., image frames), or groups of missing lines, respectively (see Figure 3). All masked pixels are then replaced by interpolated spectra from the neighboring pixels (i.e., the white pixels in Figure 3). Nearest neighbor and bilinear interpolation methods have been used for that purpose.
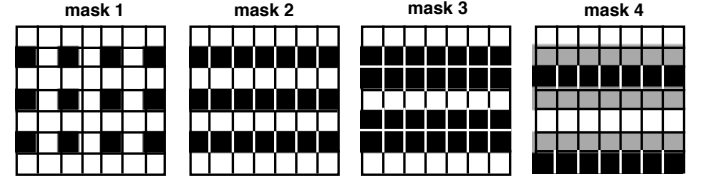

Fig. 3. Mask patterns used for resampling in the spatial dimensions. The black and greyed masked pixel positions are replaced by interpolated spectra for comparison with original data. For mask 4, the statistics are caluclated over the grey and the black area separately to simulate a the impact of a two-pixel distance of interpolation.

The systematically resampled spectra are compared to the real spectra at the very same spatial position (x,y) over the masked image areas. The mean relative deviation e_λ between the original pixels L_{xy} and the interpolated values $L_{i,xy}$ is taken as measure for the deviation which corresponds to the interpolation method:

$$e_\lambda = \left| \frac{L_{xy} - L_{i,xy}}{L_{xy}} \right|_\lambda . \qquad (4)$$

For comparison, the maximum relative error $e_{\lambda,ref}$ is defined as the mean deviation of the original image values under the mask to the average image spectrum $\overline{L}$:

$$e_{\lambda,ref} = \left| \frac{L_{xy} - \overline{\overline{L}}}{L_{xy}} \right|_\lambda . \qquad (5)$$

This value represents a global replacement of missing spectra by the mean of the image. If interpolation results are achieved close to this generic error, the interpolation obviously has failed to create an improved replacement of missing pixels.

The results from Eqs. (4) and (5) highly depend on the spatial pattern observed in the imaging spectroscopy data. We focus the analysis on the above described AVIRIS test data. This procedure is advantageous as no assumptions on the spatial distribution of distinct synthetic targets have to be taken, but rather realistic patterns of typical image scenes are set. The calculated deviations indicate which radiometric error is introduced in the data if spatial mis-registration effects are corrected by interpolation methods within 1-2 pixels distance.

The results of the analysis are summarized in Table II. The average error of the bilinear interpolation method is between 11% and 19% for the replacement of single pixels and lines, dependent on the wavelength and the interpolation method. The deviations with nearest neighbor processing are stable at about 17.5%. Bilinear interpolation performed superiorly to nearest neighbor replacement techniques by a

factor up to 2, specifically if only individual pixels have to be replaced. No significant improvement in comparison to nearest neighbor could be found for the replacement of multiple lines as for mask 3 and mask 4.

TABLE II
RELATIVE STANDARD DEVIATIONS FOR THE CORRECTION OF INCONSISTENCIES
FOR 3 INTERPOLATION METHODS, AVERAGED OVER ALL SAMPLE SCENES AND
SPECTRAL BANDS.

	Mask1	Mask2	Mask 3	Mask 4	Mask4, cent.
Image Mean	33.6%	32.8%	33.1%	32.9%	33.0%
Nearest Neighbor	17.4%	17.3%	17.4%	17.2%	17.5%
Bilinear Interpolation	11.0%	13.0%	15.3%	17.2%	19.4%

Figure 4 shows two examples of the spectral shape of the deviations. The peak at 680 nm is related to the maximal Chlorophyll absorption at this wavelength, while a trend towards larger errors is observed at longer wavelengths. The latter is related to the high variability of surface reflectance in the SWIR spectral range which is most pronounced in non-vegetated areas. If pixels in a distance larger than the pixel size have to be replaced (i.e. for center pixels of mask 4), interpolation becomes inaccurate; specifically in cities, the errors are almost on the same level as if the average spectrum would have been taken as the interpolated value. The error in nearest neighbor resampling is almost independent of the mask pattern. The difference for bilinear interpolation on the other hand is significantly lower for the replacement of pixels directly adjacent to the original values. However, the relative advantage of bilinear interpolation decreases drastically for pixels not directly adjacent to known values (black pixels of mask 4 as of Figure 3), and the trend may even be inverted for larger distance processing.
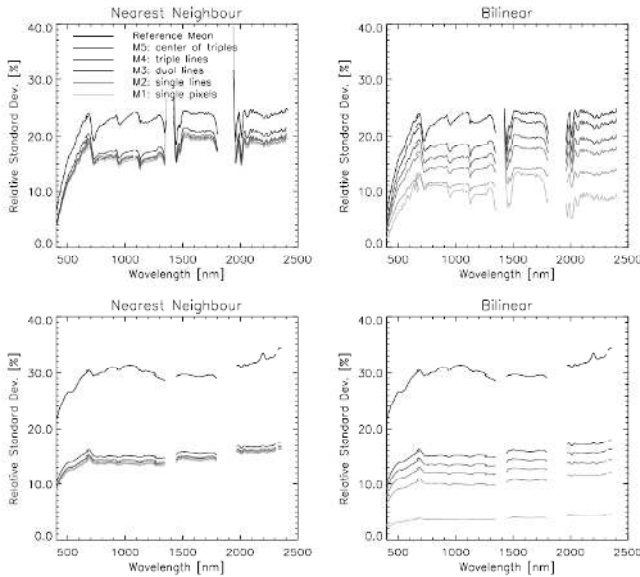

Fig. 4. Spectral variation of the deviation for the interpolation of the four mask types on two AVIRIS subsets; top: city, high altitude, bottom: geological, low altitude (the individual curves are ordered from top to bottom according to the legend).
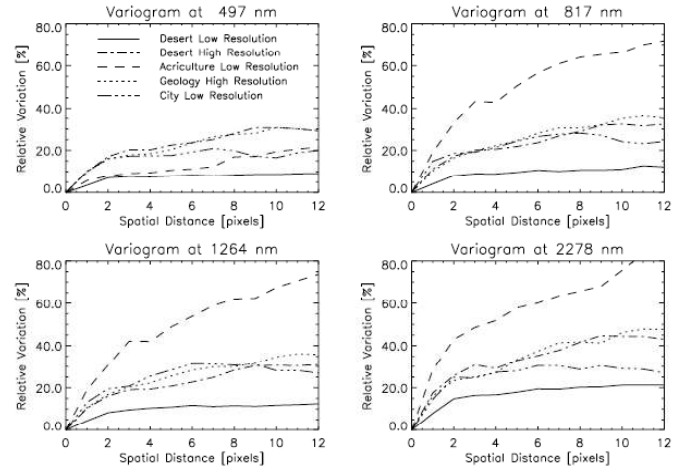

Fig. 5. AVIRIS variograms of example images at four wavelengths, plotted as distance dependent relative standard deviation.

The strong decline of dependency with increasing pixel distance is corroborated by the variograms of the imagery. The spatial dependency within a spectral band is visualized by the graphs of Figure 5 for five example scenes. The respective relative standard deviation describes the distance-dependent average deviation between compared pixel values. The relative difference is in the range of 10% for one pixel distance while it grows up to 30% for 5 pixels and more. The variogram shows for the given scene that the spatial dependencies are within up to 5 pixels. Longer distances show almost no further increase in variance and therefore the respective distant pixel values are basically independent of the starting pixel (except for agricultural fields). The higher variability for longer wavelength is directly related to the above described data instrinsic increase of surface reflectance variability. This relation also implies that interpolation only is meaningful for a distance of 1 to 5 pixels. For higher distances, any replacement method will not perform much better than an arbitrary average spectrum.

Linear interpolation is directly related to information loss. The amount of information in imaging spectroscopy data can roughly be related to the relative standard deviation. We therefore compared the standard deviations between the original and the interpolated imagery. As expected, nearest neighbor resampling retains the statistics well and does not significantly change the standard deviation in the resampled image. When linear interpolations are applied, the standard deviation is reduced by an amount of 1.9 - 3.2% as average of all data sets, depending on the mask. This loss in information leads to reduced sensitivity in image analysis. Specifically, the detection of spectral signatures in individual pixels (e.g., for geological or urban applications) is substantially affected by such information loss.

B. PSF Width Variation Effects

The band-to-band variations of the spatial PSF width (at full width half maximum; FWHM) and position are analyzed with respect to its impact on radiometric deviations from a perfectly uniform product. The PSF width of a pushbroom instrument can be non-uniform in four senses:

- In the across track direction, the along/across track spatial PSF width variations leads to non-uniformity of the spatial resolution,
- in the spectral direction, spatial PSF variations lead to non-uniformity of the acquired spectra, and
- in the across track direction, the spectral PSF width may vary.
- in along track direction, both spatial and spectral PSF may theoretically vary if the system performance stability is affected by temperature or pressure dependencies.

As mentioned earlier, we focus on the variations of the spatial PSF, while the spectral dimension is not analyzed. For pushbroom instruments, the spatial PSF width is ideally 1.0, and typically is slightly blurred to higher values, assuming a contiguous sampling [38]. The development phase of the APEX sensor has shown that the along track PSF width is more stable than the across track PSF width. Based on the observed order of magnitude for the APEX system, we investigate a variation of the PSF width of 1 to 1.6 pixels in across track direction and 1.2 to 1.6 pixels in the along track dimension across the full spectral range . For simulation of the corresponding effects, all test data sets are systematically convolved to these standard PSF values and the RMS deviation from the maximal PSF is derived.

TABLE III
RMS DEVIATIONS DUE TO PSF WIDTH VARIATIONS WITH RESPECT TO A SYMMETRIC GLOBAL MAXIMUM OF 1.6 PIXELS WIDTH AT FWHM.

across track / along track	mean deviation: AVIRIS low altitude	mean deviation: AVIRIS high altitude	mean deviation artificial	**mean deviation, real data**	overall mean; corrected
1.00/1.20	5.4%	3.7%	10.5%	**4.4%**	< 0.1%
1.25/1.35	2.8%	2.0%	5.6%	**2.3%**	<< 0.001%
1.50/1.50	0.8%	0.6%	1.5%	**0.7%**	~0%

The results of these calculations are summarized in Table III. The differing spatial patterns of the underlying data is well visible in the table: the higher resolution of low altitude imagery increases the errors significantly (from 2.3% to 4.4% in average)– this indicates that highest resolution imagery (as from APEX) will cause even more pronounced effects. For comparison, the artificial spatial pattern of the library cube results in a very high sensitivity up to 10%. When correcting the calculated values to the broadest, "worst case" PSF (see procedure described in section VI-B), the observed deviations can mostly be reduced below significant values (i.e., below 0.1%). The spectral shape of the effects from a distortion from a symmetric 1.6 pixels to 1.25/1.35 pixels PSF width is shown in Figure 6. The observed errors show the same qualitative shape as described in the previous section – except the artificial cube is differing by higher deviations and stronger discrepancies at lower wavelengths.
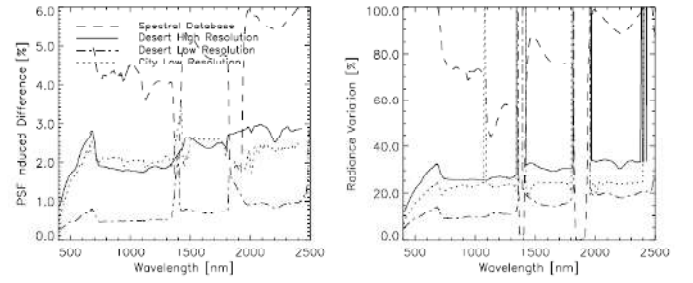

Fig. 6. PSF induced difference for four exemplary types and a PSF width variation from 1.6/1.6 to 1.25 along track and 1.35 across track. The relative variation of image radiance (standard deviation / image mean) is given in the right graph.

C. Geometric Co-Registration Effects

Another issue to be analyzed separately is the spatial co-registration between detectors (i.e., an offset between distinct optical channels). This offset is simulated by defining two distinct sensor models, which are then applied in a simulated scan over the test image scenes. The convolution is done on the simulated at-sensor radiance spectra for the artificial cube of 3x3 patches and on the AVIRIS test data sets, respectively.

For the artificial data, the at-sensor radiance data is first convolved to the mean along/across track 2D-PSF of the sensor. Registered pixels are then derived from the such degraded data by linear interpolation (see Figure 7): first, a sensor model of 1000 across track pixels is put in a straight line on this pattern, covering one pixel along track and 998 pixels across track. Second, the co-registration offset (effective in across track direction only) is added to the sensor model and a second interpolation is performed using this second sensor model. The standard deviation of the difference of these two interpolates is then taken as measure for the co-registration error. A number of 40 image lines is taken for the 3x3 pixels case. These image lines cover almost the whole spectral database with its broad variety of realistic spectra. For AVIRIS data, 150 lines have been selected within the subset images, resulting in 150'000 test spectra for each scene.
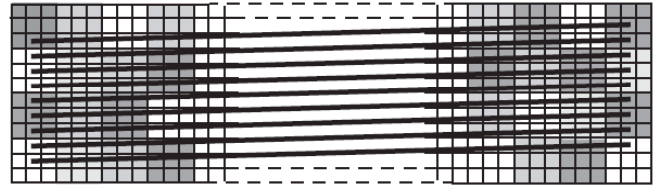

Fig. 7. Mis-registration analysis scheme on an artifical data cube with 3x3 pixels per spectrum. A sensor model (thick black lines depict scanned image lines) tilted by one pixel along track and stretched by 2 pixels across track is put on top of the artificial at-sensor radiance data.

The co-registration effect is quantified as the standard deviation of the difference between the resampled imagery using the ideal and the distorted sensor model at a distortion of 0.1 and 0.5 pixels, respectively. Relative differences of at-sensor radiance reaching 10% are observed between the two sensor models for the artificial data (see Figure 8). A first order correction is then applied to the data stemming from the mis-registered sensor model by linear interpolation in across-track direction. The linear interpolation reduces the error to a level of 2% (see Table IV). This error might be further

reduced by using dedicated interpolation routines [39]. However, our tests using deconvolution methods or quadratic interpolation routines did not lead to significantly improved results.

TABLE IV
MIS-REGISTRATION RELATED DEVIATIONS BEFORE AND AFTER INTERPOLATION.

RMS values	no interpolation 0.1 pixel	after linear interpolation 0.1 pixel	no interpolation 0.5 pixel	after linear interpolation, 0.5 pixel
low altitude	0.9%	0.4%	4.2%	1.3%
high altitude	0.7%	0.3%	3.6%	1.0%
high altitude, cities	1.0%	0.5%	4.9%	1.6%
real data, overall	1.1%	0.5%	5.1%	1.5%
artificial data	2.0%	1.0%	9.7%	2.5%

If the mis-registration analysis is performed on AVIRIS data, the absolute deviation values are lower than on the artificial data but generally show the same spectral dependencies as depicted in Figure 8. Much larger influences are observed in highly structured AVIRIS data (e.g., cities), while low resolution natural scenes are less sensitive.
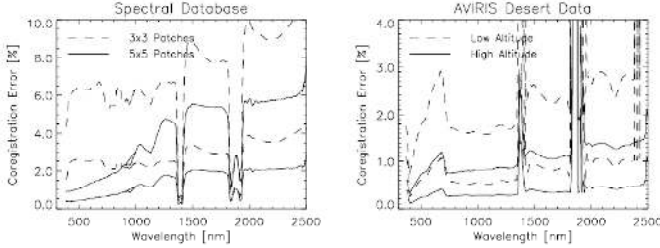

Fig. 8. Relative difference (relative standard deviation) between original and misregistered image data. The respective lower curves are the remaining errors after linear interpolation to correct for the co-registration error.

D. Keystone Effects

Within the area of a detector, the spatial and spectral mis-registration (i.e., keystone and smile) are major artefacts in pushbroom imaging spectroscopy data [2]. For APEX, both effects are expected to be below 0.2 pixels in both the visible and the short wave infrared detector. In AVIRIS data, keystone and smile are (theoretically) non-existent, although recent studies have shown some minor smile effects in AVIRIS data [9]. The expected radiometric effects of the (spatial) keystone variations are directly related to the errors described in the previous Sections V-A and V-C with the only difference that sub-pixel interpolations substitute the analyzed inter-pixel interpolations.

No separate analysis on this matter is therefore done in this paper, but a linear scaling of the derived errors with interpolation distance is done to derive the magnitude of errors: if scaling the error as summarized in Table II linearly to the expected 0.2 pixels, the deviations are in the range of ±1-2%. The same order of magnitude of the error at 1.5-2% can be derived if the values from Table IV at 0.5 pixels mis-registration are scaled to the 0.2 pixels mis-registration limit. Also, the interpolation results from Table IV are principally transferable and suggest that residual errors in a range of 0.3% are left in the data even after bilinear resampling within each frame.

VI. RECOMMENDATIONS FOR CORRECTION OF SPATIAL PSF NON-UNIFORMITY EFFECTS

A. Spatial Discontinuities Correction

The analysis of typical semi-variograms of airborne imaging spectroscopy data (compare Figure 5) shows high correlation of spectra only within 1-3 pixels distance. Therefore, interpolations beyond a distance of 3 pixels are not recommended for the correction of missing pixels. This recommendation is corroborated by the analysis of Section V-A, where a distance of 2 pixels interpolation distance showed already significant errors. The correction of spatial discontinuities shall therefore be introduced as a standard step in the preprocessing of APEX data[15] considering this criterion. However, it is yet to be analyzed if interpolation in the spectral dimension instead of the spatial dimension would lower the related errors.

B. PSF Width Correction

A possible method to correct for PSF width variations is a degradation (i.e., smoothing) of the imagery to a uniform response on the basis of the broadest PSF occurring in the image. The correction equation may be written such that:

$$L_{uniform}(\lambda_i, \theta_k) = \frac{L(\lambda, \theta) + w_{\lambda,i}\overline{L(\lambda)} + w_{\theta,k}\overline{L(\theta)}}{1 + w_{\lambda,i} + w_{\theta,k}} , \quad (6)$$

where $\overline{L(\lambda)}$ and $\overline{L(\theta)}$ are the averaged radiances in both dimensions within a local range of 3 pixels. The coefficients w are weighting factors which take into account the relative radiometric difference of the current pixel explicit PSF width and the worst case PSF of detectors. They are defined as:

$$w_i = (PSF_{worst} - PSF_i)/PSF_i , \quad (7)$$

where PSF_{worst} and PSF_i are the integrated areas under the broadest (worst case) PSF and the pixel PSFs, respectively. The weights are close to zero for the positions with large PSF widths. By this routine, uniformity is achieved while loosing a significant amount of information.

C. Geometric Co-Registration Correction

Uniformity of spectral and spatial samples is achieved by a transformation of the data from arbitrary positions *(y,z)* on the detector plane to regularly gridded (λ, θ) coordinates. Technically, this transformation involves a standard coordinate transformation and a resampling of the observed radiances in the wavelength and across-track directions [16]. The uniformity requirement demands that the band centers (λ) values be constant in the across track (θ) direction and vice versa. The grid is chosen such that the errors induced by the re-sampling are minimized, ensuring that the average deviation of from the (λ, θ) values of the actual detector pixels is minimal. Such coordinate transformation can handle arbitrary target grids. Thus, it can be used to obtain uniform radiance products across both detectors.

Given the derived order of magnitudes in this paper, such correction is required as soon as the co-registration is worse than 0.2 pixels. In this case, the target grid is chosen

such that the grid's deviation from the actual θ values of both detector's pixels is minimal at the same time. A uniform product may then be created in one single coordinate transformation step (including correction of keystone and co-registration effects). The disadvantage will be relatively high interpolation distances and the related loss of information. An alternative option is the treatment of co-registration effects in the orthorectification processing step [40] using distinct sensor models for each detector array in the geometric procedure. This bears the major advantage of one single resampling step for correcting both the spatial mis-registration and the geometric rectification.

D. Keystone Correction

For a separate keystone correction, uniform target grids are found for each detector. These grids will ultimately be visible in the radiance product as the nominal (λ, θ) grids of an instrument. When correcting the keystone effect, the observed radiance is resampled in the wavelength and across track angle directions simultaneously. For such processing, the functions $y_i(\lambda, \theta)$ and $z_k(\lambda, \theta)$, describing the relation between detector coordinates (y_i, z_k) and the nominal grid (λ, θ), need to be known exactly from laboratory calibration (see [16] for further details about this procedure).

Based on the findings in this paper, such correction is recommended for keystone variations above 0.15 pixels where the expected errors due to keystone effects surpass a critical limit of 1%. The spectral dimension has not been analyzed in this paper; nevertheless a one-step correction in both dimensions is highly recommended, as the data has been recorded in this standard frame at the same time.

VII. CONCLUSIONS

The analyses of effects due to spatial PSF non-uniformity has shown significant problems in pushbroom imaging spectroscopy data. This paper gives an order of magnitude for the expected radiometric errors if linear interpolations are used for the correction of such effects. The values have been derived from exemplary real imaging spectroscopy data and thus are only of limited generic validity. However, due to a representative selection of scenes and sensors we do not expect other orders of magnitude of the errors if the same analyses would be applied for different sensor configurations. In short, the following details have been found:

- discontinuities may be replaced to a distance not higher than 2-3 pixels by interpolation,
- the error level of any reconstruction process for missing pixels is in the range of 10-20% - if done in the spatial dimension,
- an advantage of linear interpolation over nearest neighbor resampling was shown in radiometric accuracy of the resampled spectra,
- the information loss by interpolation routines in a 1 pixel distance is significant,
- a spatial co-registration offset of 0.5 pixels leads to errors in the magnitude of 10% across the whole spectral range,

which needs to be corrected by interpolation methods,
- a critical limit to have radiometric errors below 1% is at keystone effects of 0.1 - 0.2 pixels, and
- even after interpolation of co-registration errors, a residual deviation in the range of 1 - 2% is expected, which has to be treated as a radiometric error due to spatial PSF non-uniformity.

The results of these experiments are in partial contradiction to a strong argument in imaging spectroscopy that no 'artificial' interpolated spectra shall be produced by spatial resampling. A significant higher error in the spectra derived by nearest neighbor resampling is observable in comparison to linear interpolation at one pixel distance. This difference is higher over natural areas while for man-made landscapes and spatially highly resolved image pictures, nearest neighbor methods perform almost as good as interpolations. A strong physical relation of spectra measured in a distance within the PSF width (i.e., one pixel) is inherent to the imaging system as pushbroom systems are slightly oversampled. Interpolates within this distance have a physical meaning since they are a simple weighted average of various measurements. The physical usefulness of the spectra may even be increased after such interpolations, in a sense that the spatial PSF non-uniformities no longer cause the radiometric errors as described in this paper.

While the full costs in loss of information are still to be analyzed, a first analysis in this paper has shown a 2% reduction of the standard deviation within imaging spectroscopy cubes when interpolating 25% of all pixels in an image within 1 pixel distance. The question remains, how valuable is the higher information content in non-interpolated imagery if compared to the better spatial PSF uniformity of the corrected imagery. The answer is application-dependent: while certain spectroscopic processing methods (such as linear spectral unmixing) require a spatially uniform spectrum for accurate operation, the identification of individual absorption features (such as for geological feature detection) may be done with a small portion of a spectrum. Therefore, it is recommended to provide the choice of non-uniform and uniform data products to data end users.

It has been shown that linear interpolation of pixels outside the reach of the pixel's PSF (i.e., 1.5 - 2 pixels) is questionable and should be avoided. We recommend interpolation of missing pixels only to distances within the reach of a pixel PSF – any higher distance interpolation is better done by nearest neighbor resampling or the respective pixels have to be left blank and clearly marked in a data product. If gaps in the data acquisition occur, they therefore shall not be larger than 2 pixels in diameter. This constraint has two implications: stabilizing systems for an airborne instrument should have sufficient stability such that the sensor movement during the image scan process will not lead to undersampling of more than 2 pixel size's distance. Furthermore, blind pixels on the detector and line failures shall be isolated (maximally 2 pixels diameter) – if they occur at all. Note that these results are also valid if evaluating ideal resampling approaches for geometric

rectification of any airborne scanner system and already have been considered in the implementation of the ortho–rectification method in PARGE [40].

All analyses confirmed the fact that any interpolation reduces the radiometric accuracy significantly and therefore optimal sensor design should always have priority over post-processing methods. The herewith derived spectrally dependent errors are useful for the definition of specification for upcoming instruments as well as for the definition of a processing chain. Recommendations of keystone specification can be derived from the values given in this paper, while the correction of smile artefacts needs future in-deep analysis in the spectral domain [41]. Also, the differences of various interpolation methods on the data calibration process needs to be further analyzed in future development work. Forprocessing chains of airborne imaging spectrometers, it can be concluded that in addition to the resampled orthorectified data products, non-resampled uniform or even partially non-uniform data products should be generated to avoid the radiometric errors related to any resampling step.

REFERENCES

[1] R. A. Schowengerdt, *Remote sensing: models and methods for image processing*, 2nd Ed., Academic Press, New York, 1997.

[2] P. Mouroulis, R. O. Green, and T. G. Chrien, "Design of pushbroom imaging spectrometers for optimum recovery of spectroscopic and spatial information," *Appl. Opt.*, Vol 39(13), 2000, pp. 2210-2220.

[3] B.-C. Gao, M. J. Montes, and C. O. Davis, "Refinement of wavelength calibrations of hyperspectral imaging data using a spectrum-matching technique," *Remote Sens. Environ.*, Vol. 90(4), 2004, pp. 424-433.

[4] L. Guanter, R. Richter and J. Moreno, "Spectral calibration of hyperspectral imagery using atmospheric absorption features," *Appl. Opt.*, Vol. 45(10), 2006, pp. 2360-2370.

[5] M. Rast and J. L. Bezy, "ESA's Medium Resolution Imaging Spectrometer (MERIS): mission, system and applications," in *Im. Spec. of the Terrestrial Environment*, G. Vane, ed., Proc. SPIE 1298, 1990, pp. 114-125.

[6] G. Levrini G. and S. Delvart (Eds.), *MERIS product handbook*, Version 1.3, European Space Agency, ESA, 2004.

[7] F. Rojas, R. Schowengerdt, and S. Biggar, "Validation of the on-orbit modulation transfer function for the Moderate Resolution Imaging Spectroradiometer (MODIS-AM) using on-orbit calibration data and high contrast imagery," in Proc. IGARSS 2002, IEEE, Toronto, CA, 2002, Vol. II, pp. 973–975.

[8] P. S. Barry, J. Shepanski J., and C. Segal, "HYPERION on-orbit validation of spectral calibration using atmospheric lines and an on-board system," in *Imaging Spectrometry VII*, S. M. Descour, ed., Proc. SPIE 4480, 2001, pp. 231-241.

[9] A. Wilson, W. Mockridge, and M.-C. Robinson, 1997, "Post-processing to achieve radiometric and geometric correction of ATM and CASI data." *in Proc. 3rd Int. Airb. R. S. Conf. and Exh.*, ERIM, Copenhagen, DK, 1997. Vol. I, pp. 447–454.

[10] M. Demirhan, A. Ozpinar, and L. Ozdamar, "Performance evaluation of spatial interpolation methods in the presence of noise," *Int. J. Remote Sens.*, Vol. 24, 2003, pp. 1237-1258.

[11] S.-N. Lam, "Spatial Interpolation Methods: A Review, " *The American Cartographer*, Vol. 10(2), 1983, pp. 129-149.

[12] K. I. Itten, M. Schaepman, L. De Vos, L. Hermans, H. Schlaepfer, and F. Droz, "APEX-Airborne Prism Experiment: A New Concept for an Airborne Imaging Spectrometer," in *Proc. 3rd Int. Airb. Remote Sens. Conf. and Exh.*, ERIM International Inc., Copenhagen, DK, 1997. Vol. I, pp. 181-188.

[13] J. Nieke, K. I. Itten, J. W. Kaiser, D. Schläpfer, J. Brazile, W. Debruyn, et al., "APEX: Current Status of the Airborne Dispersive Pushbroom Imaging Spectrometer" in *Earth Observing Systems IX*, W. L. Barnes and J. J. Butler Eds., Proc. SPIE 5542, 2004, pp. 109-116.

[14] D. Schläpfer and M. Schaepman, "Modelling the noise equivalent radiance requirements of imaging spectrometers based on scientific applications," *Appl. Opt.,* OSA, Vol. 41(27), 2002, pp. 5691-5701.

[15] D. Schläpfer, J. W. Kaiser, J. Brazile, M. E. Schaepman, and K. I. Itten, "Calibration concept for potential optical aberrations of the APEX pushbroom imaging spectrometer," in *Remote Sensing, Sensors, Systems, and Next Generation Satellites VII,*.R. Meynard ed., Proc. SPIE 5234, 2003, pp. 221-231.

[16] J. W. Kaiser, D. Schläpfer, J. Brazile, P. Strobl, M. E. Schaepman, and K. I. Itten, "Assimilation of Heterogeneous Calibration Measurements for the APEX Spectrometer," in *Remote Sensing, Sensors, Systems, and Next Generation Satellites VII,*.R. Meynard ed., Proc. SPIE 5234, 2003, pp. 211-220.

[17] B. Likar, J. Derganc, and F. Pernus, "Segmentation-based retrospective correction of intensity non-uniformity in multi-spectral MR images," in *Medical Imaging 2002, Image Processin*. M. Sonka, Ed., Proc. SPIE 4684, 2002, pp 507-517.

[18] J. W. Stayman and J. A. Fessler, "Regularization for uniform spatial resolution properties in penalized-likelihood image reconstruction," *IEEE Transactions on Medical Imaging*, Vol. 19(6), 2000, pp. 601-615.

[19] K. A. Peker and A. Divakaran, "Framework for measurement of the intensity of motion activity of video segments, " *Journal of Visual Communications and Image Representation*, Vol. 15(3), 2003, pp. 265-284.

[20] M. Nishihama, R. Wolfe, D. Solomon, F. Patt, J. Blanchette, A. Fleig, and E. Masuoka, *MODIS Level 1A earth location algorithm theoretical basis document*. Version 3.0, SDST-092, GSFC, 1997.

[21] J. Boardman, "Precision geocoding of low altitude AVIRIS data: lessons learnt in 1998, " in *8th Ann. JPL Airborne Earth Science Workshop*, R. Green, ed., JPL, Pasadena, CA, JPL 99-17, 1999, pp. 63-68.

[22] Y. Carmel, D. J. Dean, and C. H. Flather, "Combining location and classification error sources for estimating multi-temporal database accuracy," *PE & RS*, July 2001, pp. 865-871.

[23] D. B. Kidner, "Higher-order interpolation of regular grid digital elevation models," *Int. J. Remote Sens.*, Vol. 24(14), 2003, pp. 2981-2987.

[24] G. Moddel, "Fractional bandwidth normalization for optical spectra with application to the solar blackbody spectrum," *Appl. Opt.*, Vol. 40(3), 2001, pp. 413-416.

[25] J. Secker, K. Staenz, P. Budkewitsch, and R. A. Neville, "A vicarious calibration of the PROBE-1 hyperspectral sensor," in *Proc. 4th Int. Airb. R. S. Conf. and Exh.*, ERIM, Ottawa, CA, Vol. II, pp. 75-82, 1999.

[26] R. Bindschadler and H. Choi, "Characterizing and correcting Hyperion detectors using ice-sheet images," *IEEE Transactions on Geoscience and Remote Sensing*, Vol. 41(6), 2003, pp. 1189-1193.

[27] P. A. Burrough and R. A. McDonnell, *Principles of geographical information systems*. University Press, Oxford, 1997.

[28] R. Franke, "Scattered data interpolation: tests of some methods," *Mathematics of Computation*, Vol. 38(157), 1982, pp. 181-200.

[29] I. Admiror, "Scattered data interpolation methods for electronic imaging systems: a survey," *J. Electron. Imaging*, Vol. 11(2), 2002, pp. 157-176.

[30] S. Park and R. Schowengerdt, "Image reconstruction by parametric cubic convolution," *Computer Vision, Graphics & Image Processing*, Vol. 23, 1983, pp. 258-272.

[31] M. D. Buhmann, "Radial basis functions," *Acta Numerica*, Vol. 9(00), 2000, pp. 1-38.

[32] J. Haber, F. Zeilfelder, O. Davydov, and H.-P. Seider, "Smooth approximation and rendering of large scattered data sets," in *IEEE Visualization 2001*, T. Ertl et al., eds., IEEE Computer Society, Vol. 571, 2001, pp. 341-347.

[33] J. P. Rigol, C. H. Jarvis, and N. Stuart, "Artificial neural networks as a tool for spatial interpolation," *Int. J. of Geographical Information Science*, Vol. 15(4), 2001, pp. 323-343.

[34] R. O. Green, M. L. Eastwood, C. M. Sarture, T. G. Chrien, M. Aronsson, B. J. Chippendale, et al., "Imaging spectroscopy and the Airborne Visible/Infrared Imaging Spectrometer (AVIRIS)," *Remote Sens. Environ.*, Vol. 65(3), 1998, pp. 227-248.

[35] S. Bojinski, M. Schaepman, D. Schläpfer, and K. I. Itten, "SPECCHIO: a spectrum database for remote sensing applications," *Computers & Geosciences*, Vol. 29, 2003, pp. 27-38.

[36] A. Berk, L. S. Bernstein, G. P. Anderson, P. K. Acharya, D. C. Robertson, J. H. Chetwynd, and S. M. Adler-Golden, "MODTRAN cloud and multiple scattering upgrades with application to AVIRIS," *Remote Sens. Environ.*, Vol. 65(3), 1998, pp. 367-375.

[37] H. H. Kieffer, "Detection and correction of bad pixels in hyperspectral sensors," in *Imaging Spectrometry IV*, S. Shen, ed., Proc. SPIE 2821, 1996, pp. 93-108.

[38] F. Rojas, R. A. Schowengerdt, and S. F. Biggar, "Early results on the characterization of the Terra MODIS spatial response," *Remote Sens. Environ.*, Vol. 83, 2002, pp. 50-61.

[39] P. A. E. Janssen, *Deconvolution of images and spectra*. Academic Press, San Diego, 1997.

[40] D. Schläpfer and R. Richter, "Geo-atmospheric processing of airborne imaging spectrometry data. Part 1: Parametric Ortho-Rectification Process," *Int. J. Remote Sens.*, Vol. 23(13), 2002, pp. 2609-2630.

[41] D. Schläpfer, M. Schaepman, and P. Strobl, "Impact of spatial resampling methods on the radiometric accuracy of airborne imaging spectrometer data," in *Proc. 5th Int. Airb. R. S. Conf. and Exh.*, VERIDIAN, San Francisco / Miami, CD-ROM, 2001, 8 p.

Klaus I. Itten received the MSc and PhD degrees in Geography from Zurich University, Zurich, Switzerland in 1969 and 1973, where since 1982 he is professor in geography and remote sensing. As head of the Remote Sensing Laboratories his research and teaching interests are remote sensing and image processing for natural resources inventorying and monitoring. In particular the application of optical remote sensing, high spatial and spectral resolution image data and analysis are the focus of his research. As PI for the APEX project, imaging spectroscopy and spectro-radiometry have become important parts of his endeavours.

Daniel Schläpfer received the MSc degree in geography in 1994, the PhD (Dr.sc.nat.) in 1998, and the teaching degree in physics and geography in 1999 from the University of Zürich. His major fields of research are atmospheric and geometric preprocessing of hyperspectral data.

He has now a research associate position at the Remote Sensing Laboratories of the University of Zürich as processing scientist for ESA's Airborne Prism Experiment (APEX) and as a consultant for imaging spectroscopy projects. In addition he holds a physics teaching position at Kantonsschule Wil, Switzerland. His current scientific work focuses on the implementation of sophisticated tools for the processing and validation of image spectrometry data. He owns and runs the company 'ReSe Applications Schläpfer' which is focused on the development and distribution of the imaging spectroscopy software packages PARGE, MODO, and ATCOR.

Jens Nieke received a M. Eng. degree after studies of aeronautical and astronautical engineering at Technical University of Berlin, Germany and INSA de Lyon, France. In 1995 he joined the German Aerospace Center in Berlin (Germany) working in the MOS-IRS team, which launched a spaceborne imaging spectrometer in 1997. In 2001 he received his PhD from Technical University of Berlin on an advanced satellite mission study for regional coastal zone monitoring. From 2000 until 2003, Jens Nieke worked as Visiting Scientist at JAXA EORC, Tokyo, Japan. His tasks covered algorithm development, data analysis, calibration of ground-truth instruments and conducting ground-truth experiments for the ADEOS-II GLI mission.
In 2004, he joined Remote Sensing Laboratories of the University of Zürich, where he is employed as senior scientist, lecturer and project manager of the APEX ESA project. Frequently, he is involved as visiting professor in the lecturing program of various Universities, such as Chiba University, Japan or International Space University, France.